Int. J. Electrochem. Sci., 7 **(2012)** 9560 - 9572

International Journal of
ELECTROCHEMICAL
SCIENCE
www.electrochemsci.org

Plasmon Enhanced Photoelectrochemical Activity of Ag-Cu Nanoparticles on TiO_2 /Ti Substrates

Jian Liu and Fuyi Chen[*]

State Key Laboratory of Solidification Processing, Northwestern Polytechnical University, Xian, 710072, China
[*]E-mail: fuyichen@nwpu.edu.cn

Received: 15 August 2012 / *Accepted:* 10 September 2012 / *Published:* 1 October 2012

Ag-Cu nanoparticles were deposited on titania nanotube arrays via photodeposition method. The photocurrent density and voltage curves were measured under simulated sunlight and visible light irradiation conditions. Ag-Cu co-deposited photoelectrodes with a mole ratio of 1 to 4 exhibited the highest short-circuit photocurrent (J_{SC}) under both irradiation conditions. The Mott-Schottky analysis indicates that the Ag-Cu decorated photoelectrodes were more sensitive in the visible light region, and the electron injection efficiency was relatively higher than that of the pure Ag or Cu decorated photoelectrodes. The Schottky barrier analyses indicate that the photoexcited electrons transferred from metal nanoparticles to TiO_2.

Keywords: photoelectrochemistry; TiO_2 nanotube; Ag-Cu nanoparticle; Mott-Schottky;

1. INTRODUCTION

Metal (such as Au, Ag, and Cu) nanoparticles exhibit significant optical absorption and scattering properties due to the existence of a localized surface plasmon resonance (LSPR), where the resonance wavelength depends on the size, shape, and dielectric environment around the nanoparticles [1-3]. The plasmon resonance has been applied in the field of imaging [4], biosensors [5, 6], and surface-enhanced Raman scattering [7, 8]. More recently, plasmon absorption of metal nanoparticles combined with TiO_2 is applied to photovoltaic devices [9, 10] and photocatalysts [11, 12], and an enhanced light harvesting property and a visible-light-induced charge separation were obtained for the benefit of the metal nanoparticles.

However, several different explanations have been presented about the role of metal nanoparticles in the observed improvement in light conversion efficiency. These include (i) metal nanoparticles increased absorption due to surface plasmons and light trapping effects [13], (ii) metal

nanoparticles functioned as electron donor to promote electron transfer from metal to semiconductor [9, 10, 14] and (iii) metal nanoparticles served as electron trapping media that can minimize the surface charge recombination in semiconductor [15, 16]. Meanwhile, two main mechanisms were mentioned for the electron transfer between the metal nanoparticle and the semiconductor during the energy conversion process. First, Tatsuma et al. [9, 10, 17] and other workers [14, 18] proposed that the photoexcited electrons in the metal nanoparticles transfer from the metal nanoparticles to the TiO_2 conduction band since the photoresponse of these metal-TiO_2 composite films was consistent with the absorption spectra of Au or Ag nanoparticles. Second, Kamat et al [15, 16] and Li et al. [19] suggested that the noble metal nanoparticles could act as electron sinks or traps in the metal-TiO_2 nanostructures so as to accumulate the photogenerated electrons, which can minimize charge recombination in the semiconductor films. Obviously, a better understanding of these effects was crucial in exploiting the beneficial aspects of metal nanoparticles in photovoltaics.

In this paper, TiO_2 nanotube arrays used as the substrate were obtained from the anodization of titanium, which can reduce the scattering of free electrons and enhance electron mobility [20]. We chose the bimetallic Ag-Cu nanoparticles as the plasmonic medium where Cu alloying was used to prevent the natural oxidation of the Ag nanoparticles in solution and keep its good plasmonic property, and their absorption spectra are different from those of individual Ag or Cu [21]. It has been previously reported that chemical method [22], electrodeposition [23] and UV photo reduction [24] of two metal salts have been used for the preparation of the bimetallic nanoparticles. Here, photodeposition was used to synthesis Ag-Cu nanoparticles on the TiO_2 nanotube arrays to obtain the AgCu-TiO_2/Ti photoelectrodes, and their photoelectrochemical properties were measured under simulated sunlight and visible light. The Mott-Schottky analyses indicate that the electron injection and light-harvesting efficiencies were improved for the Ag-Cu decorated photoelectrodes.

2. MATERIALS AND METHODS

2.1 Preparation of TiO_2 nanotube layers

TiO_2 nanotube layer were prepared via rapid anodic oxidation method [25]. The titanium foils (99.9%, 50 mm × 10 mm × 2 mm) were mechanically polished with sandpaper and chemically polished in 1M HF for 2 min. Then the polished titanium foils were cleaned with acetone, ethanol, and distilled water by ultrasonic bath, respectively. Finally the titanium substrates were anodized using direct current voltage source (AAP 150V DC POWER SUPPLY) consisting of a two-electrode configuration with a piece of platinum foil (10 mm × 10 mm) as cathode. Electrolytes were 0.3M NH_4F + 0.03M Na_2CO_3 + 3 vol% H_2O in ethylene glycol. The anodization process was carried on under constant direct current potential 80 V, which was achieved by a ramp from 0V to 80V with a sweep rate of 0.5 V/s. The anodization process was carried out at 283K in the cold water bath and the time was set to 320 seconds. When the anodization step finished, the samples were rinsed with distilled water and dried in air, and then annealed at 773 K for 1.5 h in an atmosphere to obtain crystalline phase.

2.2 Photodeposition of Cu, Ag, and Ag-Cu nanoparticles

0.1 M $Cu(CH_3COO)_2$ and 0.1 M $AgNO_3$ aqueous solutions were prepared and mixed with ethanol, respectively, with a volume ratio of 1 to 20. 1 mL mixed solutions were cast on the surface of TiO_2 nanotube layer which had been washed in acetone, ethanol, and distilled water by ultrasonic bath. During photodeposition, mixed solutions on the substrates were irradiated with 365 nm UV light with the incident power of 140 mW/cm^2 for 300s. The first UV irradiation was to promote the nucleation of Cu and Ag ions, and then the second UV irradiation was designed to control the growth of Cu and Ag nanoparticles. The irradiation power is 14mW/cm^2 and the irradiation time were 300s, 600s and 900s, the corresponding samples were labeled Cu-300s, Cu-600s, Cu-900s, Ag-300s, Ag-600s, and Ag-900s.

The electrolytes for the photodeposition of Ag-Cu nanoparticles were consisted of three different molar ratio of Ag to Cu, *i.e.*, 4:1, 1:1, and 1:4, and the total concentration of Cu and Ag cations is 0.1 M, which was diluted with ethanol by the volume ratio of 1 to 20. During the deposition process, TiO_2 nanotube layer with 1 mL electrolyte cast on were UV irradiated under 140 mW/cm^2 for 300s, and 14 mW/cm^2 for 900s, after UV irradiation, the samples were washed with the deionized water immediately. The corresponding samples were labeled AgCu 4:1, AgCu 1:1, and AgCu 1:4.

2.3 Characterization and analysis

The surface morphologies of samples were characterized by scanning electron microscopy (JSM, 6390A) with energy dispersive X-ray spectroscopy (SEM-EDS). The electrochemical properties were tested by an Electrochemistry Station (CHI 660C) in a solution of 1 mM sodium sulfate (Na_2SO_4) in the dark, visible light or simulated solar light from a 300 W Xenon lamp with the 100 mW/cm^2 intensity. Before the test, the samples were sealed with epoxy, left the portions covered with nanoparticles exposed and the exposed area was about 0.1256 cm^2. The photocurrent density - voltage curves (J-V) were measured at a potential sweep rate of 10 mV/s, with the Pt net as counter electrode, and a saturated calomel electrode (SCE) as reference electrode. Mott-Schottky experiments were conducted to evaluate the capacitance behavior under DC potential polarization. The potential range was -0.8 to +0.8 V_{SCE} with potential steps of 10 mV at a constant frequency of 1000 Hz.

3. RESULT AND DISCUSSION

3.1 Morphological features

The TiO_2 nanotube layers prepared by the rapid anodic oxidation have a nanotube length of *ca.* 3.1 μm (inset of the Fig. 1a). The surface morphology of the Cu, Ag and Ag-Cu nanoparticles deposited on TiO_2 nanotube layers were shown in Fig. 1(a-c), Fig. 1(d-f) and Fig. 1(g-i), respectively. As shown from Fig. 1(a) to Fig. 1(c), the Cu nanoparticles were evenly and densely distributed on the surface of TiO_2 nanotube layer, the measured nanoparticle size ranged 46 nm to 120 nm, nanoparticles size didn't grow evidently when the irradiation time increased from 2 to 3 times. From Fig 1(d) to (f),

obviously, the Ag nanoparticles are bigger than Cu nanoparticles and are not in uniform size with the big ones over 500 nm and the small ones below 100 nm.

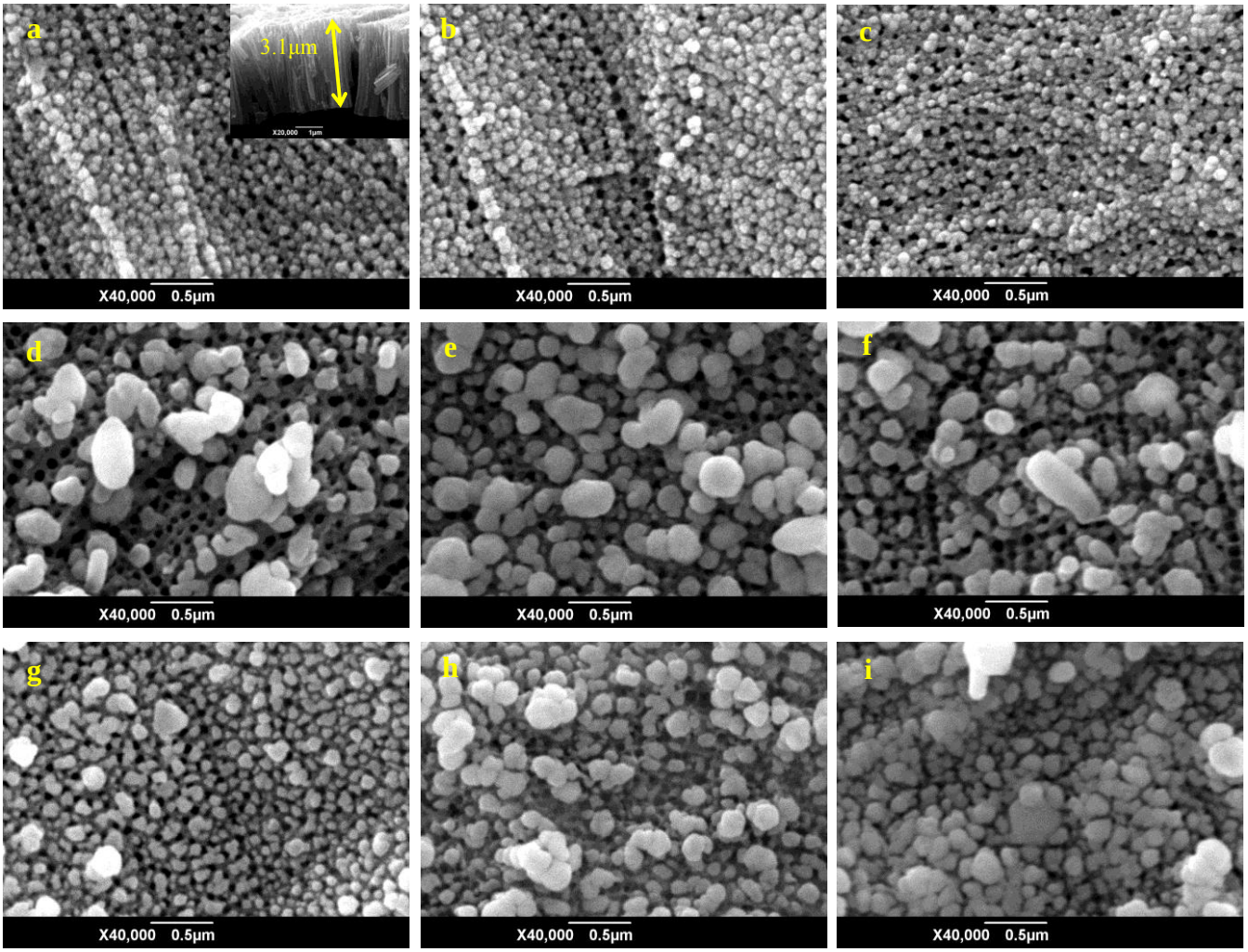

Figure 1. SEM images of the Cu, Ag and Ag-Cu nanoparticles deposited on TiO_2 nanotube layers in samples of (a) Cu-300s, (b) Cu-600s, (c) Cu-900s, (d) Ag-300s, (e) Ag-600s, (f) Ag-900s, (g) AgCu4:1, (h) AgCu1:1, and (i) AgCu1:4.

The possible reason is that the standard electrode potential of Ag^+/Ag^0 (0.78 eV) is higher than that of Cu^{2+}/Cu^0 (0.34 eV), so Ag^+ is reduced more rapidly and grows faster than Cu^{2+}. On the other hand, CH_3COO^- can be complex with Cu^{2+} cations and also a good hole-consuming sacrificial agent [26], therefore, the CH_3COO^- can promoted the Cu^{2+} nucleation in the first stage and the growth process was inhibited because of the consumption of Cu^{2+}. On the other hand, since the NO_3^- can not consume holes, the number of nucleation of silver is less and the density of Ag nanoparticles is lower than the Cu nanoparticles'.

Fig. 1(g) to (i) shows the surface morphology of the Ag-Cu nanoparticles on TiO_2 nanotube layers, it is obvious that the Ag-Cu nanoparticles were denser than Ag nanoparticles, and this can be ascribed to the existence of CH_3COO^-. The energy dispersive X-ray spectroscopy (EDS) show that the

atom ratios of Ag to Cu are 2.51:0.07, 2.75:0.45 and 1.68:3.72 for samples of AgCu 4:1, AgCu-1:1, and AgCu 1:4, respectively. The Cu content was less than that in the electrolyte because of that the reduced Cu can be further oxidized by Ag^+.

3.2 The current density and voltage (J-V) curves

Table 1. J_{SC} (mA/cm^2) values of pure TiO_2 layer and Cu, Ag, AgCu-TiO_2/Ti photoanodes

Electrodes	TiO_2 layer	Cu-300s	Cu-600s	Cu-900s	Ag-300s	Ag-600s	Ag-900s	AgCu 4:1	AgCu 1:1	AgCu 1:4
Simulated sunlight	-0.272	-0.546	-0.709	-0.861	-1.115	-0.674	-0.727	-0.399	-0.786	-1.201
Visible light	-0.057	-0.190	-0.396	-0.407	-0.377	-0.193	-0.188	-0.184	-0.374	-0.734

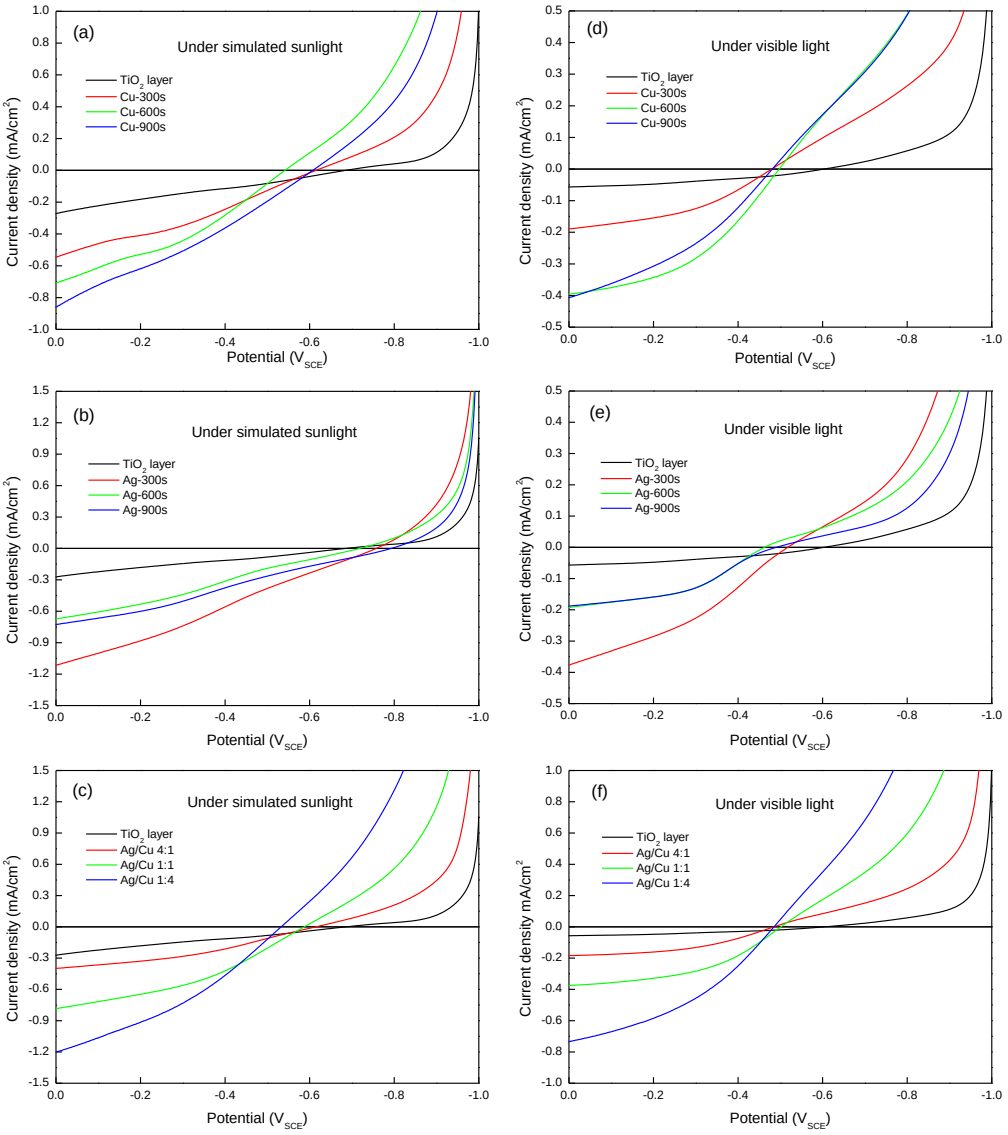

Figure 2. The current density and voltage (J-V) curves for the pure TiO_2/Ti and the Cu, Ag, AgCu-TiO_2/Ti photoelectrodes measured under simulated sunlight (a, b, c) and under visible light (d, e, f).

Fig. 2 (a)~(c) show the J-V curves measured under simulated sunlight and the corresponding results are listed in table 1. All the samples decorated with Cu, Ag, and Ag-Cu nanoparticles have higher values of J_{SC} than pure TiO_2 substrate, which indicates that the deposition of Cu, Ag, and Ag-Cu nanoparticles enhanced the photovoltaic properties of TiO_2 nanotube layers. This can be explained by Eq.1 [27]:

$$J_{SC} = \int_0^{d_{PE}} i_g(\lambda, x)dx = q\phi(\lambda)\eta_{LH}(\lambda)\eta_{inj}(\lambda) \qquad (1)$$

where i_g is the current density per unit volume, x the distance from the photoelectrode substrate, q elementary charge, Φ the incident spectral photon flux, η_{LH} the light-harvesting efficiency, and η_{inj} the electron injection efficiency. From Eq. 1, we can see that improved J_{SC} will be obtained by enhancing the values of η_{LH} and η_{inj}. Actually, the metal nanoparticles deposited on the surface of TiO_2 will shift the valence band and the conduct band to lower energy, which improves the light-harvesting capacity [28]. Furthermore, the deposition of metal nanoparticles will also decrease the charge transfer resistance and enhance the electron injection efficiency.

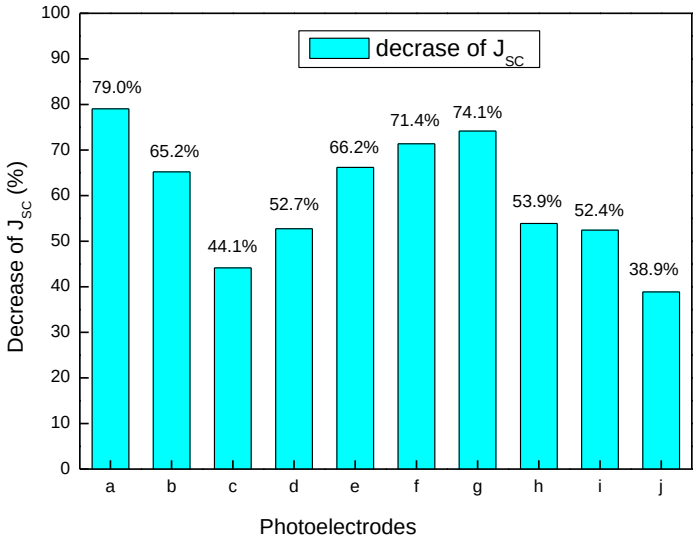

Figure 3. The decreased J_{SC} measured under visible light in compare with that measured under simulated sunlight for photoelectrodes of (a) pure TiO_2/Ti, (b) Cu-300s, (c) Cu-600s, (d) Cu-900s, (e) Ag-300s, (f) Ag-600s, (g) Ag-900s, (h) AgCu4:1, (i) AgCu1:1, and (j) AgCu1:4.

The J_{SC} of the Cu-TiO_2/Ti photoelectrode increased as the photodeposition time grows. This can be attributed to that more Cu nanoparticles were deposited on the substrate without evidently increasing diameter, which lead to the increase of the light absorption. The highest value of J_{SC} was obtained by Cu-900s, which is -0.861 mA/cm^2. This value is close to the highest J_{SC} (-1.115 mA/cm^2) obtained by Ag-300s among the Ag decorated samples. These results indicate that Cu may potentially be used to replace the more expensive metal of Ag for the decoration of TiO_2 for solar cell

applications. While for the Ag-TiO_2/Ti photoelectrodes, long time deposition lead to a decrease of J_{SC}. The reason may be that the Ag nanoparticles are so large (>100 nm) that much more lights were scattered than that were absorbed [29]. Among all the photoelectrodes, as shown in Table 1, the AgCu 1:4 sample got the highest J_{SC} value, which is -1.201 mA/cm^2. This may be benefit from its relatively small nanoparticles which avoid backscattering too many lights and the special properties of the AgCu alloy..

Fig. 2 (d)-(f) show the J-V curves measured under visible light and the corresponding results are also listed in table 1. It is obvious that the J_{SC} measured under visible light decreased in comparison with that measured under simulated sunlight for all samples. As shown in Fig. 3, the pure TiO_2 layer has the largest J_{SC} decline (79%) for that the TiO_2 was sensitive only to UV light. The J_{SC} values of the Ag-TiO_2/Ti photoelectrodes decreased by 66~74%, which is very close to that of the TiO_2 layer. For the Cu-TiO_2/Ti photoelectrodes, the highest J_{SC} is -0.407 mA/cm^2, which is larger than the highest J_{SC} (-0.377 mA/cm^2) obtained by Ag-TiO_2/Ti photoelectrodes. This means that more visible lights are absorbed by Cu-TiO_2/Ti photoelectrodes because of that the localized surface plasmon resonance (LSPR) peak of Cu nanoparticles are red-shifted and much broader than that of Ag nanoparticles [3, 30]. The AgCu 1:4 sample exhibited the highest J_{SC} of -0.734 mA/cm^2 and the lowest fall of J_{SC} of 38.9%, indicating that Ag-Cu nanoparticles are more photosensitive in the visible light region than the individual Ag and Cu nanoparticles.

3.3 Mott-Schottky

Mott-Schottky analysis was conducted in order to evaluate the effect of DC potential on the capacitance behavior of the metal loaded nanotube layer and calculate the charge carrier concentration. As shown in Fig. 4, the Mott-Schottky curves are in accordance with the expected behavior of n-type semiconductor under increased anodic bias, *i.e.* a sharp decrease in the capacitance when the anodic bias is increased above the flat band potential until a plateau in the capacitance is reached [31]. In all these studies, the Mott-Schottky curves contain two to three linear regions with a different slope, which was explained by the multiple donor states in the band gap [32, 33].

The capacitance, C_{SC}, was calculated according to Eq. 2:

$$C_{SC} = -1/2\pi fZ'' \tag{2}$$

where f is the frequency in the experiment and Z'' is the imaginary component of the impedance. According to the Mott–Schottky theory, the concentration of electron donors, N can be calculated using Eq. 3:

$$N = \frac{2C^2}{q\varepsilon\varepsilon_0 A^2 (E - E_{fb} - kT/q)} \tag{3}$$

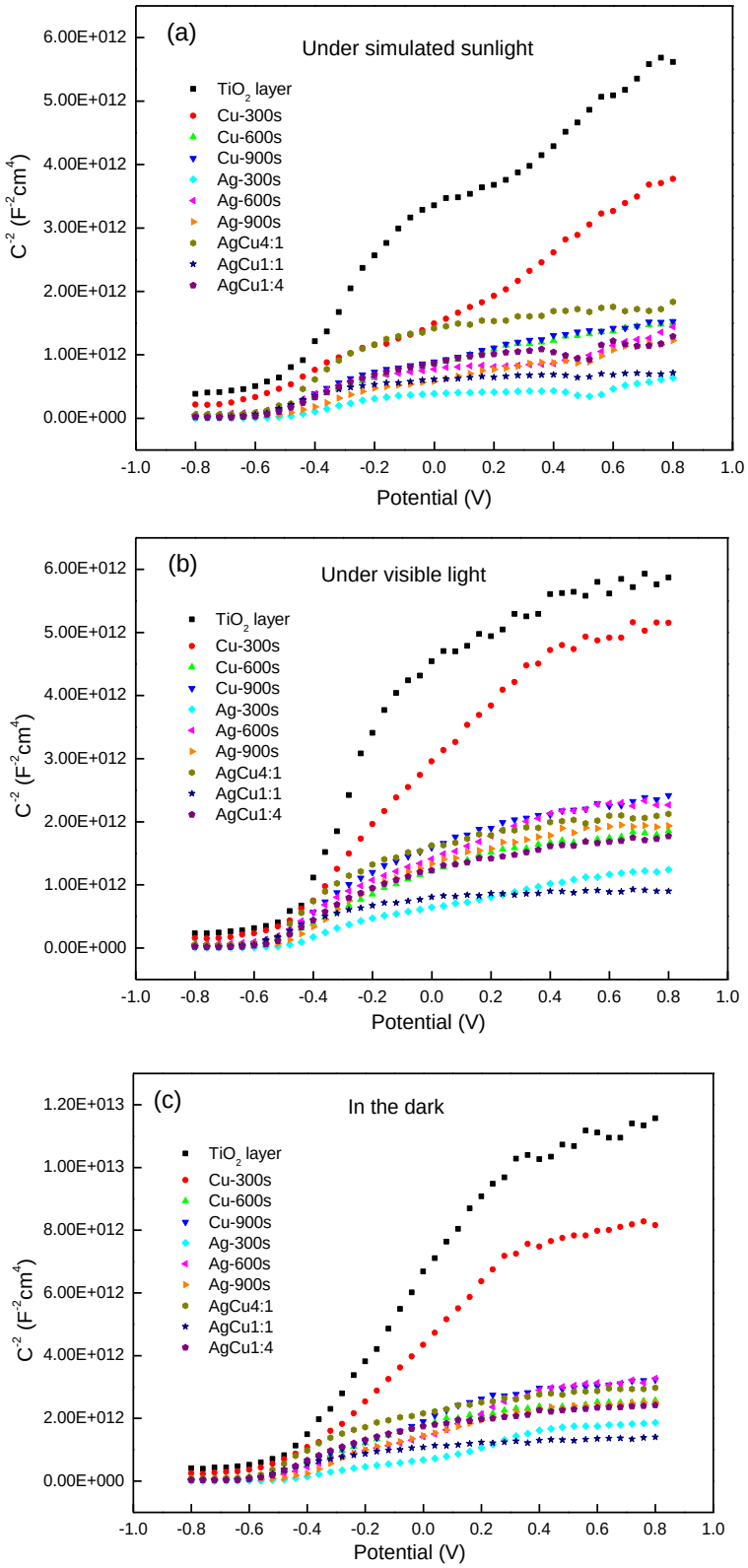

Figure 4. Mott–Schottky plots for the pure TiO_2/Ti and Cu-, Ag-, AgCu-TiO_2/Ti photoelectrodes measured under the simulated sunlight (a), under the visible light (b) and in the dark(c).

where ε denotes the TiO_2 dielectric constant (we assume ε=120 [34]), ε_0 the vacuum permittivity, q the charge of the electron, A the geometric electrode area, N the electron donor concentration, E the applied potential, E_{fb} the flat band potential and the term kT/q is 25 mV at room temperature. The values of electron donor concentration (N, calculated according to the second linear slope of the curve from the flat band potential to about -0.2 V_{SCE}) were presented in Table 2.

Table 2. Charge carrier concentration in the different photoelectrodes as derived from the Mott-Schottky analysis

Electrodes	simulated light	visible light	dark
	N (10^{19} cm^{-3})	N (10^{19} cm^{-3})	N (10^{19} cm^{-3})
TiO_2 layer	1.065	0.632	0.536
Cu-300s	3.054	1.397	0.783
Cu-600s	4.622	3.386	2.377
Cu-900s	3.420	2.087	1.785
Ag-300s	4.550	3.019	2.931
Ag-600s	3.837	2.370	2.196
Ag-900s	3.132	1.463	1.198
AgCu4:1	1.151	1.053	0.744
AgCu1:1	2.923	2.255	1.513
AgCu1:4	3.630	2.702	1.864

Comparing the values in Table 2 to that in Table 1, we can first find that J_{SC} values increase as the electron or other charge carrier concentration gains in the three different irradiation conditions, which means that the loading of metal nanoparticles on the TiO_2 nanotube layer is beneficial to the electron concentration. Secondly, under the irradiation of simulated sunlight, the Cu decorated ones have relatively high electron concentration and Ag-Cu decorated ones have the lowest values, however, the AgCu 1:4 sample exhibited the highest J_{SC}, and next is the Ag-300s and Cu-900s sample. These phenomena may be explained by that Cu nanoparticles have a good capacity to harvest light and that the electrons produced are poorly injected into the TiO_2 layers [3, 35], moreover, the high J_{SC} for the Ag-Cu photoelectrodes with low electron concentration indicates that the electron injection efficiency is high. Thirdly, for the three different irradiation conditions, the electron concentration of the Cu and Ag decorated photoelectrodes exhibit a decreasing of 26~54% from the simulated light to the visible light while the corresponding decrease of the Ag-Cu decorated ones was below 26%. This indicates that the photoelectrochemical response of the Ag-Cu decorated photoelectrode doesn't strongly depend on UV light. Additionally, the electron concentration of the Cu and Ag-Cu decorated photoelectrodes is ~30% lower in the dark than that under visible light and the Ag decorated ones are 3~18% lower. These observations demonstrate that the photoelectrodes with Ag nanoparticles loaded have a poor

light harvesting capacity in the visible region, and the Ag-Cu decorated photoelectrodes are more sensitive in visible region and can harvest more lights than the other photoelectrodes [36, 37].

3.4 Schottky barrier analysis

The work function difference between the metal and the n-TiO_2 results in electrons transferred from TiO_2 to the metal nanoparticles yielding a Schottky junction. According to the Mott-Schottky model, the Schottky barrier height (SBH) at the metal/TiO_2 interface can be related to the difference between the metal work function W_m and the electron affinity χ_s of the semiconductor by the equation $\phi_{SBH} = W_m - \chi_s$. If the photoexcited electron transfers from the metal nanoparticles to the TiO_2, W_m will become larger, and the ϕ_{SBH} will increase.

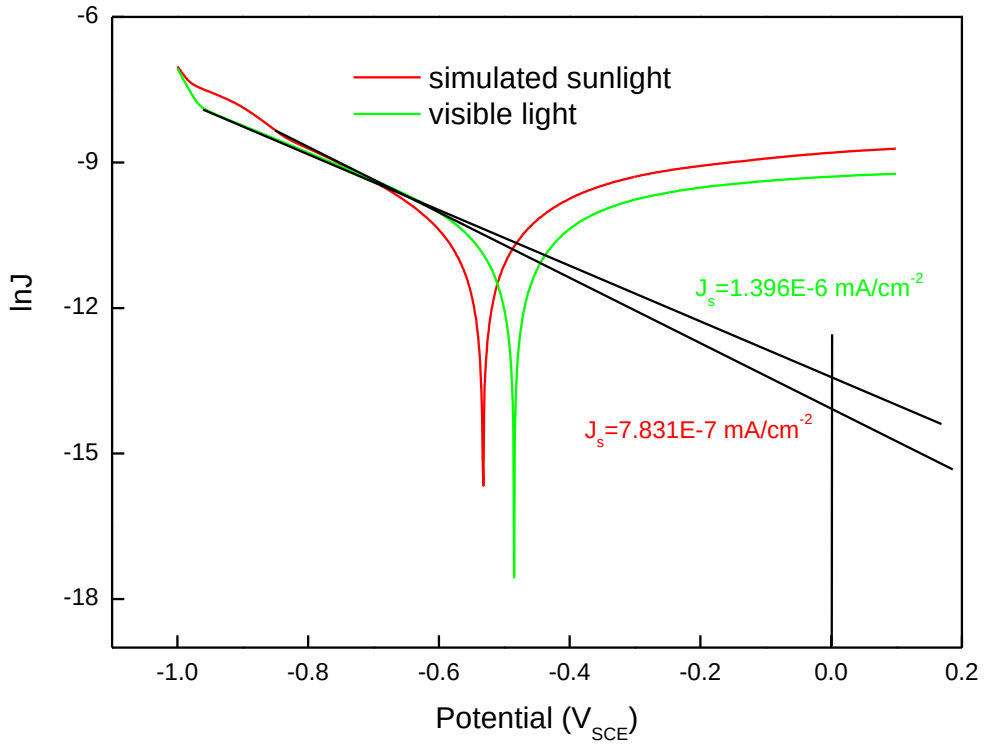

Figure 5. The current density and voltage (J-V) curves for the photoelectrode AgCu 1:4 measured under visible light and simulated sunlight. The linear part of the *lnJ-V* extrapolates to *V=0* V_{SCE} and yields J_s as the dark line shows.

Therefore, we can determine the electron transport direction by comparing the SBH changes under different irradiation conditions. The SBH values were calculated in lnJ-V diagram shown in Fig. 5 by Eq. 4 [38]:

$$J_S = A^* T^2 \exp(-q\phi_{SBH} / k_B T) \quad (4)$$

where ϕ_{SBH} is SBH at the zero bias, A^* is the Richardson constant, k_B is the Boltzmann constant, and J_s is the zero bias saturation current density. The calculated SBH values were presented in Table 3.

Table 3. ϕ_{SBH} (eV) values of the photoelectrodes under simulated sunlight and visible light

Electrodes	TiO_2 layer	Cu-300s	Cu-600s	Cu-900s	Ag-300s	Ag-600s	Ag-900s	AgCu 4:1	AgCu 1:1	AgCu 1:4
Simulated sunlight	1.293	1.096	1.053	1.081	1.203	1.165	1.282	1.082	1.054	1.021
Visible light	1.101	1.004	1.003	1.016	1.072	1.057	1.095	1.019	1.013	1.006

As shown in Table 3, the TiO_2 substrate has the largest decrease of SBH (0.192 eV), since that most of the electrons are excited by UV light. The least decline of SBH obtained by the AgCu 1:4 is 0.015 eV, which means that the AgCu-TiO_2/Ti photoelectrode is less sensitive to UV light and that more electrons were produced under visible light. The large decrease of the SBH values of the Ag-TiO_2/Ti photoelectrodes again manifests that the poor light absorption property of Ag nanoparticles in visible region. The ϕ_{SBH} values of the Cu, AgCu-TiO_2/Ti photoelectrodes are very close, indicating that the Cu component have a dominated effect on the photoelectronic properties of Ag-Cu nanoparticles. It's worthy to note that the decrease of the SBH corresponds to that of the J_{SC}. This also well explained the good photoelectrochemical performance of the photoanode AgCu 1:4 under visible light irradiation. In addition, all the ϕ_{SBH} values calculated under the simulated sunlight are higher than that measured under visible light, which was attributed to the transportation of the excited electrons to the TiO_2 conduct band. This result clearly indicates that the metal nanoparticles can be photoexcited as electron donors, and that the electrons transferred from metal nanoparticles to TiO_2, which is agreeable with Tatsuma and his co-workers' view [9, 10, 17].

The high J_{SC} value and electron injection efficiency in the visible region of Ag-Cu nanoparticle decorated photoelectrode may be caused by the special electron transport mechanism between Ag-Cu nanoparticles and TiO_2 substrate. We assumed that Cu has a broad absorption in the visible light and Ag is good for electron injection. Therefore, the electrons were photoexcited when the visible light irradiated on the Cu nanoparticles and then fast transferred to the Ag nanoparticles. In this process, the electron concentration may become low for the charge recombination, but the high injection efficiency will make up this part of electron loss since the fast electron injection from the Ag nanoparticles into TiO_2 conduct band.

4 CONCLUSIONS

Cu, Ag, and Ag-Cu nanoparticles were deposited on the TiO_2/Ti substrates via photodeposition method. The AgCu1:4 sample got the highest J_{SC} both under simulated sunlight and visible light

irradiation. The Mott-Schottky and Schottky barrier height analysis indicated that the AgCu-TiO_2/Ti photoanodes are more sensitive to visible light and have higher electron injection efficiency than the individual Ag- or Cu-TiO_2/Ti electrodes. We also clearly identified that the photoexcited electrons transferred from the metal nanoparticles to TiO_2 layer from the Schottky barrier analysis. Finally, a possible electron transport mechanism is presented.

ACKNOWLEDGEMENTS

This study was supported by the National Natural Science Foundation of China (Grant Nos. 51271148 and 50971100), the Research Fund of State Key Laboratory of Solidification Processing in China (Grant No. 30-TP-2009), and the NPU Foundation for Fundamental Research (Grant No. NPU-FFR-JC200931).

References

1. X. Lang, L. Qian, P. Guan, J. Zi, M. Chen, *Appl. Phys. Lett.*, 98 (2011) 093701
2. J.C. Heckel, G. Chumanov, *J. Phys. Chem. C*, 115 (2011) 7261–7269
3. E. Kazuma, T. Yamaguchi, N. Sakai, T. Tatsuma, *Nanoscale*, 3 (2011) 3641-3645
4. I.H. El-Sayed, X. Huang, M.A. El-Sayed, *Nano Lett.*, 5 (2005) 829–834
5. J. Homola, Anal. Bioanal. Chem., 377 (2003) 528–539
6. J.C. Trefry, J.L. Monahan, K.M. Weaver, A.J. Meyerhoefer, M.M. Markopolous, Z.S. Arnold, D.P. Wooley, I.E. Pavel, *J. Am. Chem. Soc.*, 132 (2010) 10970–10972
7. P. Hildebrandt, M. Stockburger, *J. Phys. Chem.*, 88 (1984) 5935–5944
8. M. Muniz-Miranda, C. Gellini, E. Giorgetti, *J. Phys. Chem. C*, 115 (2011) 5021–5027
9. Y. Tian, T. Tatsuma, *Chem. Commun.*, 16 (2004) 1810–1811
10. Y. Tian, T. Tatsuma, *J. Am. Chem. Soc.*, 127 (2005) 7632–7637
11. K. Awazu, M. Fujimaki, C. Rockstuhl, J. Tominaga, H. Murakami, Y. Ohki, N. Yoshida, T. Watanabe, *J. Am. Chem. Soc.*, 130 (2008) 1676–1680
12. H. Irie, K. Kamiya, T. Shibanuma, S. Miura, D.A. Tryk, T. Yokoyama, K. Hashimoto, *J. Phys. Chem. C*, 113 (2009) 10761–10766
13. H.R. Stuart, D.G. Hall, *Appl. Phys. Lett.*, 73 (1998) 3815-3817
14. S. Mubeen, G. Hernandez-Sosa, D. Moses, J. Lee, M. Moskovits, *Nano Lett.*, 11 (2011) 5548–5552
15. N. Chandrasekharan, P.V. Kamat, *J. Phys. Chem. B*, 104 (2000) 10851–10857
16. A, Takai, P.V. Kamat, *ACS NANO*, 5: (2011) 7369-7376
17. N. Sakai, Y. Fujiwara, Y. Takahashi, T. Tatsuma, *ChemPhysChem.*, 10 (2009) 766 – 769
18. A. Furube, L. Du, K. Hara, R. Katoh, M. Tachiya, *J. Am. Chem. Soc.*, 129 (2007) 14852-14853
19. L. Liu, G, Wang, Y. Li, Y. Li, J.Z. Zhang, *Nano Res.*, 4 (2011) 249–258
20. D.W. Gong, C.A. Grimes, O.K. Varghese, W.C. Hu, R.S. Singh, Z. Chen, E.C. Dickey, *J. Mater. Res.*, 16 (2001) 3331-3334.
21. G. Li, Y. Luo, *Inorg. Chem.*, 1 (2008) 360-364
22. V.V. Agrawal, P. Mahalakshmi, G.U. Kulkarni, C.N. Rao, *Langmuir*, 22 (2006) 1846-1851
23. B. Wickman, Y.E. Seidel, Z. Jusys, B. Kasemo, R.J. Behm, *ACS NANO*, 5 (2011) 2547–2558
24. J. Herrmann, J. Disdier, P. Pichat, A. Fernandez, A. Gonzalez-Elipe, G. Munuera, C. Leclercq, *J. Catalysis*, 132 (1991) 490–497
25. Y. Wang, Y. Wu, Y. Qin, G. Xu, X. Hu, J. Cui, H. Zheng, Y. Hong, X. Zhang, *J. Alloys Compd.*, 509 (2011) L157–L160
26. S. Yamazaki, S. Iwai, J. Yano, H. Taniguchi, *J. Phys. Chem. A*, 105 (2001) 11285-11290

27. K. Miettunen, J. Halme, A. Visuri, P. Lund, *J. Phys. Chem. C*, 115 (2011) 7019–7031
28. Z. Zhang, W. Tang, M. Neurock, J.T. Yates, *J. Phys. Chem. C*, 115 (2011) 23848–23853
29. D. Derkacs, S.H. Lim, P. Matheu, W. Mar, E.T. Yu, *Appl. Phys. Lett.*, 89 (2006) 093103
30. G.H. Chan, J. Zhao, E.M. Hicks, G.C. Schatz, R.P. Van Duyne, *Nano Lett.*, 7 (2007) 1947–1952
31. L.V. Taveira, A.A. Sagüés, J.M. Macak, P. Schmuki, *J. Electrochem. Soc.*, 155 (2008) C293–C302
32. N. Baram, Y. Ein-Eli, *J. Phys. Chem. C*, 114 (2010) 9781–9790
33. H. Tsuchiya, J.M. Macak, A. Ghicov, H.S. Rader, L. Taveira, P. Schmuki, *Corros. Sci.*, 49 (2007) 203–210
34. L. Kavan, M. Grazel, *Electrochim. Acta*, 40 (1995) 643–652
35. H. Jiang, K. Moon, C. P. Wong, *Advanced Packaging Materials: Processes, Properties and Interfaces*, (2005) 173–177
36. G. Suyal, *Thin Solid Films*, 426 (2003) 53–61
37. M. Tsuji, S. Hikino, R. Tanabe, M. Matsunagaa, Y. Sano, *CrystEngComm*, 12 (2010), 3900–3908
38. J.H. Werner, *Appl. Phys. A*, 47 (1988) 291–300